Volume 5 | Number 8 | 21 April 2021

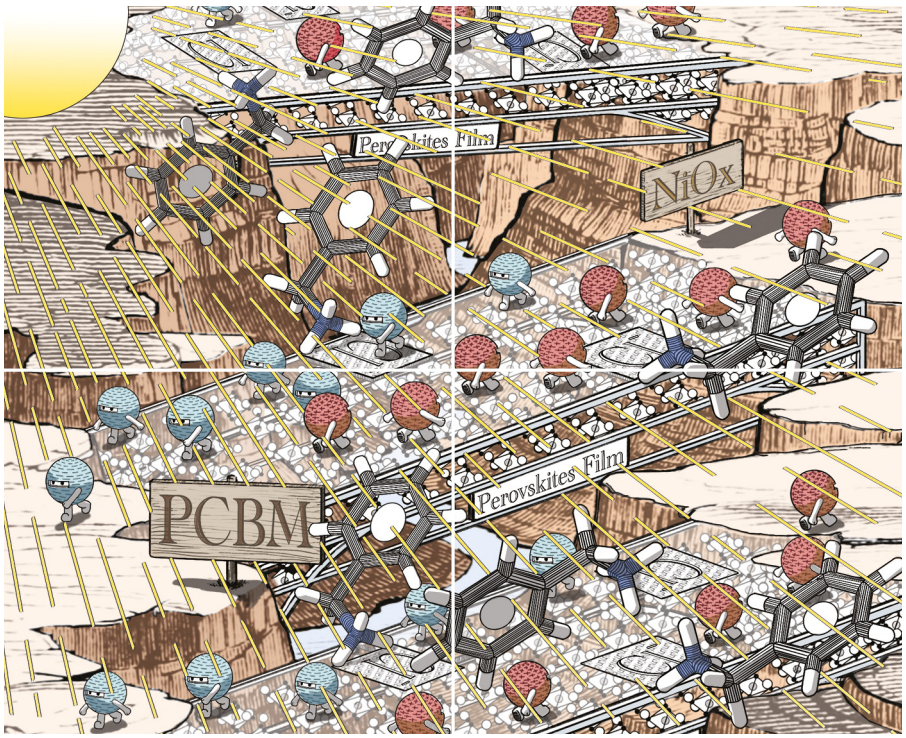

MATERIALS CHEMISTRY

FRONTIERS

CCS 中国化学会 CHINESE CHEMICAL SOCIETY
ICCAS 1956
ROYAL SOCIETY OF CHEMISTRY
rsc.li/frontiers-materials

MATERIALS CHEMISTRY
FRONTIERS

RESEARCH ARTICLE

View Article Online
View Journal | View Issue

Cite this: *Mater. Chem. Front.*, 2021, **5**, 3378

Synergistic improvements in the performance and stability of inverted planar $MAPbI_3$-based perovskite solar cells incorporating benzylammonium halide salt additives†

Hung-Cheng Chen,*[a] Jie-Min Lan,[b] Hsiang-Lin Hsu,[b] Chia-Wei Li,[b] Tien-Shou Shieh,[c] Ken-Tsung Wong *[d] and Chih-Ping Chen *[b]

In this study, three different benzylammonium halide (Cl, Br, and I) salts were investigated to elucidate their effects as additives on $MAPbI_3$ perovskite surface morphology, crystal structure, optical properties, and solar cell performance and stability. In particular, the additive benzylammonium chloride (BZACl) has a cationic benzylammonium (BZA) ion as a surface capping ligand and exhibits stronger electronegativity attributed to anionic Cl^- ions for suppressing the defect formation of iodine vacancies. The study demonstrated that most effectively reducing the defects and suppressing non-radiative recombination result in a significant increase in the photoluminescence (PL) intensity and lifetime of BZACl-doped $MAPbI_3$ thin films. By optimizing the concentration of BZACl to about 0.27 mol% relative to $MAPbI_3$, the corresponding device exhibited a maximum power conversion efficiency (PCE) of 19.8%, with negligible hysteresis (PCE = 20.4% in reverse scan), in comparison with the PCE of 17.8% for the control device with pristine perovskite films. In addition, excellent moisture stability is demonstrated with 90% retainment of the initial efficiency after 30 days of unencapsulated operation under ambient air conditions (~45% relative humidity). This work highlights the great potential of benzylammonium halide salts as additives for developing high-efficiency and simultaneously stable $MAPbI_3$-based perovskite solar cells.

Received 25th November 2020,
Accepted 19th January 2021

DOI: 10.1039/d0qm00983k

rsc.li/frontiers-materials

Introduction

Hybrid organic–inorganic perovskites (*e.g.*, $CH_3NH_3PbX_3$, X = I, Br, and Cl) possess excellent photoelectric properties including tunable optical band gap, low exciton binding energy (2–100 meV) in the 3D crystal structure, long exciton diffusion lengths (100–1000 nm), high charge carrier mobility (1–100 $cm^2\ V^{-1}\ s^{-1}$) and long charge carrier lifetime (0.1–1 μs).[1–3] Thus, the perovskite film as the photoactive layer material in solar cells has been extensively studied in the past ten years.[4] Recently, the power conversion efficiency (PCE) of single-junction perovskite solar cells (PSCs) over 25% has been realized.[5] The tremendous achievements in the device performance make perovskites as one of the most competitive materials in photovoltaic applications.[6,7]

The crystal quality and morphology of perovskite layers have greatly governed the photovoltaic performance in any type of perovskite-based device architectures.[4] Currently, the solution-processing fabrication techniques such as spin-coating, blade coating and inkjet printing are still dominant in the polycrystalline perovskite thin film deposition.[8,9] These approaches are with advantages of the low material wastage, low temperature and large-area manufacturing. However, these solution-processing methods followed by thermal annealing steps often suffer from the formation of grain boundaries and high density defects in the crystal growth.[10,11] Most studies show that defects are significantly responsible for the non-radiative charge recombination, charge trapping and the origin of the notorious current–voltage hysteresis.[12] In addition, grain boundaries have also been shown to worsen the photocurrent hysteresis and facilitate the perovskite degradation.[13] In order to eliminate defects in the perovskite or at grain boundaries, surfaces, and interfaces, several defect passivation strategies have been developed for enhancing perovskite solar cell performance and improving the device stability.[14,15]

[a] *Department of Applied Chemistry, National University of Kaohsiung, Kaohsiung 81148, Taiwan. E-mail: hcchen@nuk.edu.tw*
[b] *Department of Materials Engineering, Ming Chi University of Technology, New Taipei City 243, Taiwan. E-mail: cpchen@mail.mcut.edu.tw*
[c] *Material and Chemical Research Laboratories, Industrial Technology Research Institute, Hsinchu 310, Taiwan*
[d] *Department of Chemistry, National Taiwan University, Taipei 10617, Taiwan. E-mail: kenwong@ntu.edu.tw*

† Electronic supplementary information (ESI) available. See DOI: 10.1039/d0qm00983k

The facile and effective approaches of organic ligand passivated perovskites *via* post-treatment have been widely applied in PSCs.[16,17] For instance, phenethylammonium iodide (PEAI) was utilized for post-treatment of mixed perovskites $FA_{1-x}MA_xPbI_3$ to suppress the surface non-radiative recombination defects, and an efficiency of 23.32% was achieved in n-i-p planar PSCs recently.[5] Noteworthy, due to the strong coordination ability of ammonium group on these organic ligands, the post-treatment with excess organic cations subsequently can break the perovskite crystal structure. Thus, in the methylammonium lead iodide ($MAPbI_3$) perovskite case, the organic cation can partially replace MA^+ to form a 2D/3D mixed (or quasi-3D) perovskite structure.[18] Thus, it is conceivable that this post-treatment approach is only for the effective passivation on the perovskite surface defects and interfacial defects (*i.e.* the perovskite/HTL interface and perovskite/ETL interface), not for the ionic point defects or bulk defects inside the perovskite grains.[11,17] In order to further passivate the point defects in the perovskite lattice and reduce the grain boundaries, the additives in perovskite precursor solutions are widely adopted for depositing high-quality perovskite films and enhancing the operational stability of PSCs.[19] A great number of additives have been developed to achieve efficient and stable PSCs such as Lewis acid-based additives (*e.g.*, metal–halide salts,[20] fullerene derivatives[21]), Lewis base-based additives (*e.g.*, caffeine of O-donors,[22] dimethyl sulfide of S-donors,[23] and alkyl amine of N-donors[24]), functional organic chromophores,[25–27] ionic liquids,[28] zwitterions[29] and polymers.[30,31] Furthermore, the additives are introduced into the PSC fabrication process for giving high uniformity and low defect density of perovskite films.[32–35] More importantly, the PSCs with suitable additives showed that the moisture and thermal stability have been significantly improved.[33] Therefore, additive engineering applied to perovskite photovoltaics is capable of large-scale manufacture of high-quality perovskite films that may eventually lead to practical commercialization.[36]

In 2016, Wang *et al.* first demonstrated the excellent moisture tolerance of formamidinium lead iodide ($FAPbI_3$) films and significant reduction in *J–V* hysteresis after the perovskite layer was treated with benzylamine (BZA) for surface passivation.[37] In particular, the passivation effect using BZA is much superior to that of aniline and phenethylamine-modified perovskites. More recently, the 2D perovskite capping layers by employing (halogenated-) benzylammonium cations for photovoltaic devices with 2D/3D perovskite stacking structures have been developed.[38,39] The 2D passivation layers with hydrophobic benzylammonium-based aromatic cations not only enhance the moisture and thermal stability but also improve the performance of PSCs. This draws our attention to apply the benzylammonium cation as an additive for the acquisition of both highly efficient and stable PSCs. Although benzylammonium is the one of widely used aromatic arylammonium spacer cation reported in low-dimensional or dimensionally mixed (2D/3D) perovskites as well as the surface passivation reagent in the post-treatment process, we are surprised that benzylammonium cations as additives introduced into the 3D $MAPbI_3$ perovskite-based photovoltaic devices with inverted planar structures have not been reported so far in PSCs.[40,41]

In addition, the effective recombination centres originating from the point defects inside the perovskite grains have been widely investigated, in particular for iodine vacancy defects in bulk $MAPbI_3$.[42,43] Because chloride (Cl^-) and bromide (Br^-) ions have more electronegative and smaller ionic radius than iodine (I^-) ions, they have strong ionic bonds with Pb(II) than the Pb–I bond in the perovskite films. Therefore, in order to eliminate the nonradiative recombination centres formed by iodine vacancy, the halide-mixing perovskites with trace amounts of Cl^- or Br^- doping have been developed.[44–46] Particularly, the halide-mixing perovskites such as $MAPbI_{3-x}Cl_x$ and $MAPbI_{3-x}Br_x$ exhibited the greatest improvements in terms of carrier diffusion length, carrier lifetime and grain size of perovskite films.[47] As a result, the substitution of various amounts of I^- with Cl^- or Br^- ions not only leads to halide-mixing PSCs exhibiting better efficiency but also improves the device stability as compared with those of the $MAPbI_3$-based PSCs.[48]

To address the above-mentioned issues, in this work, we developed a series of benzylammonium (BZA^+) halide (Cl^-, Br^-, I^-) salts to perform additive engineering for efficient and stable $MAPbI_3$-based PSCs. At the low concentrations of additives, the hydrophobic capping ligand of BZA can terminate grain surfaces and effectively passivate defects on $MAPbI_3$ surfaces. Meanwhile, the Cl^- or Br^- ions doped into the $MAPbI_3$ lattice suppress the formation of iodine vacancies. As a result, the p-i-n $MAPbI_3$-based PSCs with a BZACl additive particularly exhibited fill factors up to ~80%, significantly enhancing the average PCEs from 16.94% to 19.43%. Moreover, the BZACl passivated perovskite devices also displayed a remarkable improvement in air stability. Overall, our findings show that additive engineering using BZACl provides a simple and efficient strategy to simultaneously improve the performance and stability of PSCs.

Results and discussion

The solar cell structure and the chemical structures of the processing additives are shown in Fig. 1. The p–i–n planar heterojunction PSCs were fabricated according to the device

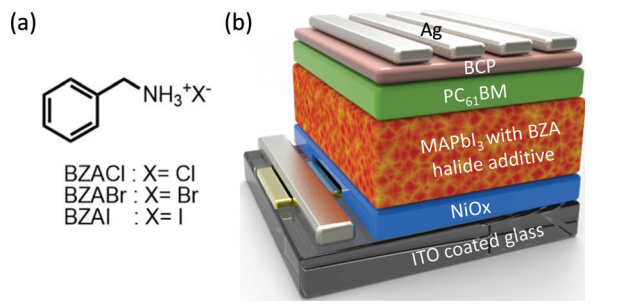

Fig. 1 (a) Chemical structures of benzyl ammonium (BZA) halide additives and (b) device configuration of the perovskite solar cell.

configuration of indium tin oxide (ITO)/NiO_X/$MAPbI_3$ (without and with BZA halide salts)/[6,6]-phenyl-C_{61}-butyric acid methyl ester ($PC_{61}BM$)/bathocuproine (BCP)/Ag, where NiO_X, $PC_{61}BM$, and BCP serve as hole transport layer, electron transport layer, and interfacial layer, respectively. The details of the device fabrication are provided in the Experimental section. We first investigated the impact of perovskite precursors without and with different concentrations (mg mL^{-1}) of BZACl on device performance. The photovoltaic parameters of the PSCs with various BZA halide salt additives and related concentrations are collected in Table S1 (ESI†). The initially scanning best-performing PSC was obtained by adding 0.5 mg mL^{-1} BZACl into the $MAPbI_3$ precursor solution containing 1.3 M of PbI_2 and MAI (1 : 1 molar ratio) in anhydrous dimethylformamide (DMF) and dimethylsulfoxide (DMSO). Further increasing the additive concentration of BZACl to 1.0 mg mL^{-1} would deteriorate device performance. Consequently, the perovskite–BZA hybrid precursor solution was prepared by dissolving the BZA halide salt additive (BAZCl, BAZBr, or BAZI) with an optimal concentration of 0.5 mg mL^{-1} in the $MAPbI_3$ precursor solution for all the characterization studies in this report. Although the larger organic cation of BZA^+ is incompatible with the 3D perovskite structure, the molar ratio of MA^+/BZA^+ is still as high as 375 herein. It suggests that a dimensionally tuned phenomenon does not occur herein. Thus, we proposed that the BZA^+ cation only plays the role of capping ligands on the perovskite surface or at the grain boundaries between the 3D perovskite crystal structure. To further elucidate the BZA halide salt additive for improving the hydrophobic property of perovskite films, we performed water contact angle measurement. As observed in Fig. S1 (ESI), pristine $MAPbI_3$ films exhibited a contact angle of 42°, whereas BZACl-doped perovskite films showed a higher contact angle of 48°, which indicates improved moisture resistance.

To investigate whether the additives would influence the structural and optical properties of the resulting $MAPbI_3$ film, the X-ray diffraction (XRD) and ultraviolet-visible (UV-vis) absorption measurements were performed to evaluate the crystalline structure of perovskite films with BZA halide salt additives, as shown in Fig. 2. For all films, the main diffraction peaks at 2θ = 14.1, 20.1, and 28.7° correspond to the (110), (112), and (220) crystal faces of tetragonal structure $MAPbI_3$, respectively.[49] These results indicate that the crystal structures of perovskite films are not affected by the BZA halide salt additives.[50] Noteworthy, as the thicknesses of all the films are similar, the intensity of these diffraction peaks in BZACl-doped films is slightly higher than that of the other films, which proves that BZACl additives could effectively improve the crystallinity of the perovskite films. The higher peak intensity in XRD patterns indicates the higher phase purity and preferential orientation of the perovskite crystals, which are beneficial to improve the electronic properties such as charge carrier transport in perovskite films. However, it is known that the optical absorption property is strongly dependent on the crystallinity of the films. Fig. 2(b) shows the UV-vis spectra of the $MAPbI_3$ films with and without the BZA halide salt additives casted on the glass/ITO/NiO_x substrates, respectively. The typical absorption spectrum of the pristine 3D $MAPbI_3$ perovskite film was shown with absorption band edge at ≈790 nm. Apparently, the absorption spectra of the perovskite films with additives depicted in Fig. 2(b) are quite similar to that of the reference pristine perovskite films. Besides, the characteristic multiple absorption peaks of the 2D films were not observed in the absorption spectra which is well consistent with the XRD results.[50] Therefore, it can be concluded that the addition of BZA halide salts did not destroy the intrinsic crystal structure of the perovskite film, which is in agreement with our assumption for the 3D crystallinity structure.

To verify the role of BZA halide salt additives in perovskite film formation, the morphological characterization was conducted by scanning electron microscopy (SEM). As shown in the top-view SEM images in Fig. 3(a)–(d), there is no significant change in grain sizes between the reference pristine perovskite film and BZA halide-doped films. All perovskite films exhibit similar average grain sizes of ∼250 nm. However, as shown in the cross-sectional SEM images in Fig. 3(e), the multiple grain packing can be clearly observed throughout the thickness of the reference pristine perovskite film. This discontinuous crystal formation could result in a disadvantageous effect on charge carrier transport and collection in the PSC devices. Oppositely, as observed from the SEM images in Fig. 3(f)–(h), the continuous grain

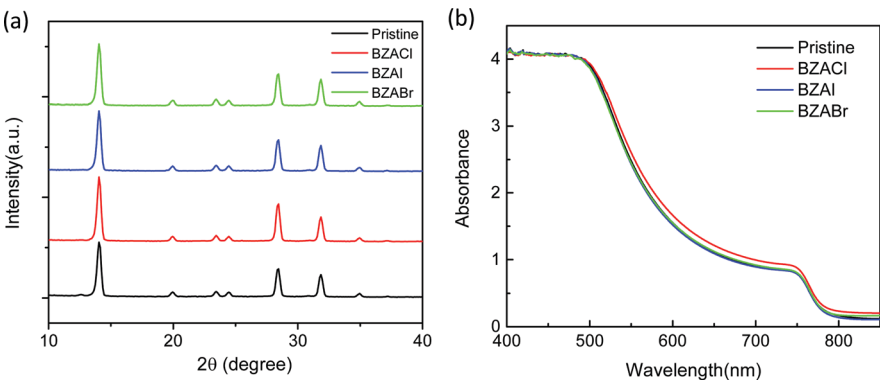

Fig. 2 Structure and optical characterization of the perovskite films w/o and with BZA halide salt additives. (a) XRD patterns and (b) UV-vis absorption spectra.

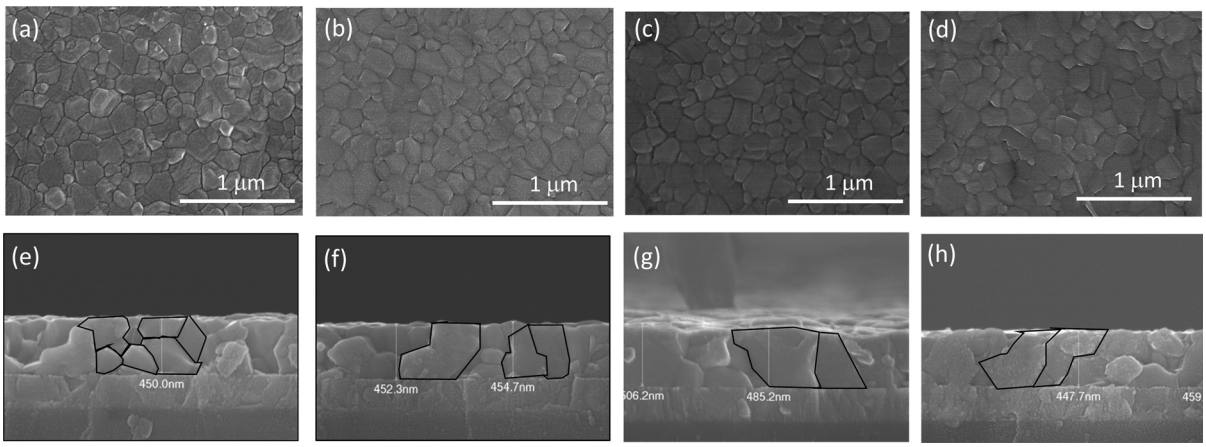

Fig. 3 Top-view SEM and cross-section SEM of the morphology of $MAPbI_3$ films w/o additives (a and e) and with BZACl (b and f), BZAI (c and g) and BZABr (d and h), respectively.

growth throughout the thickness (~450 nm) can be obtained in all the BZA halide–doped films. These results indicated that the crystals are more favourable to grow in the bottom-up direction and also weakly dependent on the halide ions (Cl^- and Br^-) of additives. Therefore, it can be concluded that the BZA^+ cation of additives could play a critical role in affecting the growth kinetics of the perovskite films.

Because the Cl^- and Br^- ion concentration of additives are much lower than the iodide ion concentration in the $MAPbI_3$ precursor solution and could probably evaporate *via* the gaseous state of methylammonium chloride ($CH_3NH_3Cl(g)$) or methylammonium bromide ($CH_3NH_3Br(g)$) formation during thermal annealing,[51,52] it is important to know the elemental distribution of halide ions in the final perovskite films. To verify whether or not the small amount of residual halide ions may still remain in the perovskite film after thermal annealing, time-of-flight secondary ion mass spectrometry (ToF-SIMS) measurements were employed to analyse the chemical composition and the vertical distribution of halide ions within the perovskite film.[53] The ToF-SIMS depth profiles along the depth direction from the top of the perovskite film down to the bottom NiO_x layer are depicted in Fig. 4. As shown in Fig. 4(b) and (c), it is clearly revealed that the Cl^- ions and Br^- ions uniformly distribute across the perovskite films, respectively. These results confirm that the Cl^- ions and Br^- ions are incorporated into the crystal lattice of the bulk $MAPbI_3$ crystal.

To investigate the passivation effect of perovskite films with BZA halide additives, the steady-state photoluminescence (PL) and time-resolved photoluminescence (TRPL) measurements were conducted to study the film quality and charge recombination dynamics, as shown in Fig. 5.[54] The steady-state PL spectra of the pristine and BAZ halide additives containing perovskite films in Fig. 5(a) do not show any noticeable shift in peak positions centred at around 770 nm, indicating that the BAZ halide additives do not affect the optical bandgap of the perovskite. Meanwhile, the greatly enhanced PL intensity can be observed in all BAZ halide additives containing perovskite films, compared with the pristine film. This result indicates that the defects in perovskites are effectively reduced and then the longer excited charge carrier lifetimes are persevered in the BAZ halide additive–containing perovskite crystals. The TRPL was measured by monitoring the peak emission at 770 nm, as shown in Fig. 5(b). The emission lifetime and fractional amplitudes were fitted using a bi-exponential decay model using the formula: $I(t) = A_1 \exp(t/\tau_1) + A_2 \exp(t/\tau_2) + B$. The fitted parameters are summarized in Table 1. The fast decay lifetime (τ_1) and the slow decay lifetime (τ_2) are attributed to the non-radiative recombination induced by charge-trapping defect states and bimolecular radiative recombination inside the grains,

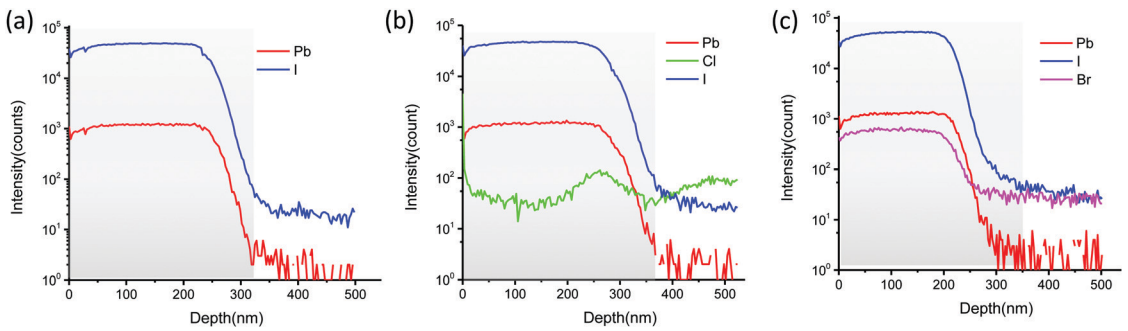

Fig. 4 ToF-SIMS depth profile of the perovskite film (a) w/o additives and with (b)BAZCl and (c)BAZBr additives.

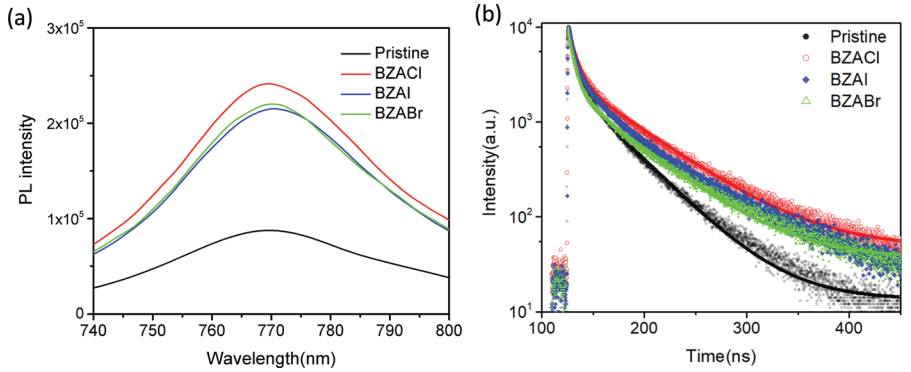

Fig. 5 (a) Steady-state PL spectra and (b) TRPL spectra of the pristine and BAZ halide additives (BZACl, BZABr and BZAI) containing perovskite films.

Table 1 Fitted parameters for the TRPL profiles using a bi-exponential decay model for the pristine and additive-containing perovskite films

Film	A_1 (%)	τ_1 (ns)	A_2 (%)	τ_2 (ns)	$\tau_{average}$ (ns)
Pristine	29.7	6.6	70.4	40.3	30.3
BZACl	22.1	7.4	77.9	56.5	45.6
BZAI	24.7	6.7	75.3	51.8	40.6
BZABr	26.3	6.8	73.7	51.6	39.6

respectively.[55] Compared with the reference pristine film, the decrease in fraction (A_1) of the faster decay components and the longer time constant (τ_1) were obtained in the all BAZ halide additive-containing perovskite films, which can be ascribed to the reduced defect density in the modified perovskite film. Furthermore, the notable increase in the fraction and the longer time constant (τ_2) were obtained in the all BAZ halide additive-containing perovskite films, which suggests significantly suppressed trap-induced nonradiative recombination losses in the perovskite layer. As a result, all the BAZ halide additive–containing perovskite films have the average carrier lifetime longer than that of the pristine film. Noteworthy, the $\tau_{average}$ is significantly enhanced from 30.3 ns of the pristine film to 45.6 ns of the BZACl additive. According to the results of the enhanced PL intensity and elongated PL lifetime in the perovskite with BZA halide additives, they further verify that BZA halide additives can effectively reduce traps and suppress charge recombination in perovskite films. In particular, the BZACl additive-containing films exhibited the longest carrier lifetime, compared to BZABr and BZAI. It can be concluded that the BZACl additive has much more efficient passivation capability to the perovskite film than that of BZABr and BZAI.

To further explore the interactions between BZA halide additives and perovskite crystals, X-ray photoelectron spectroscopy (XPS) measurements were conducted. The XPS of Pb $4f_{7/2}$ and Pb $4f_{5/2}$ core-level spectra in pristine $MAPbI_3$ films and films with BZA halide additives are shown in Fig. 6. As shown in Fig. 6, the characteristic peaks of Pb valence electrons in Pb $4f_{7/2}$ and Pb $4f_{5/2}$ of BZA halide additive-containing films exhibit obvious shifts toward higher binding energies than that of the pristine $MAPbI_3$ film. The results indicate the existence of chemical interaction between BZA halide additives and Pb(II)

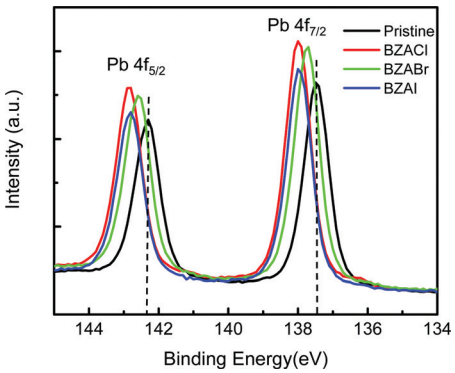

Fig. 6 XPS spectra of the Pb 4f region of pristine $MAPbI_3$ films, and films with BAZ halide additives, respectively.

in the perovskite crystal. In particular, the highest binding energy shift was observed in the film with BZACl additive. It is attributed to Cl^- with the stronger electronegativity than I^-. Thus, it can be stronger binding with the Pb(II) ion that reduces the electron density from the Pb(II) ion.[56] Similarly, it was also reported that the shift toward a higher binding energy in the Pb 4f XPS spectra was observed in $MAPbI_3$ with other chloride-containing additives.[56,57]

The charge carrier transport properties at the interface were further characterized using electrochemical impedance spectroscopy (EIS).[58] The Nyquist plots of $MAPbI_3$-based PSC devices without and with various BZA halide salt additives under AM 1.5G illumination are shown in Fig. 7. The equivalent circuit was used to fit the impedance spectra for EIS analysis comprising a device series resistance (R_s) and interfacial charge transfer resistance (R_{CT}). The fitting data are collected in Table S2 (ESI†). Noteworthy, the R_{CT} is significantly decreased from 587 Ω in a pristine $MAPbI_3$-based perovskite device to 205 Ω in perovskites incorporating BZACl additives. These results indicate that BZACl additives can effectively passivate the trap-states and grain boundaries near the perovskite/HTL interface and perovskite/ETL interface, which results in a better interface contact and more effective charge transfer in the heterojunction.[59,60]

The current density–voltage (J–V) characteristics of each champion $MAPbI_3$-based PSC device w/o and with various

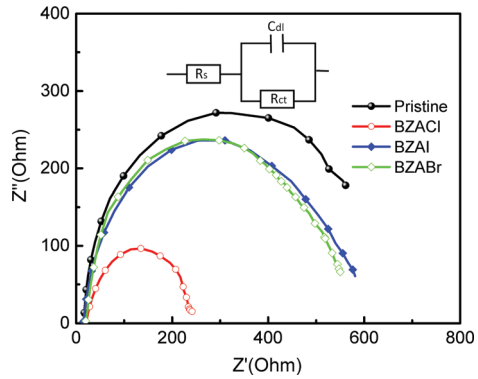

Fig. 7 Nyquist plots of perovskite devices w/o and with various BZA halide salt additives under illumination.

BZA halide salt additives under AM 1.5G simulated illumination (100 mW cm^{-2}), and statistical photovoltaic data for devices are shown in Fig. 8 and Table 2, respectively. As shown in Fig. 8, it is apparent that the *J–V* curve of the device with BZACl additives in the perovskite layer is superior to other devices. It displays a high V_{OC} of 1.10 V, a large short-circuit current density (J_{SC}) of 22.77 mA cm^{-2}, a fill factor (FF) of 79.3%, and an overall PCE of 19.8%, which is among the highest efficiencies. Moreover, the average PCEs of 17.2 ± 0.4%, 19.2 ± 0.4%, 15.7 ± 0.4%, and 16.3 ± 0.3% are obtained from the reference devices with pristine perovskite film and the device with BZACl, BZABr, and BZAI additives, respectively, showing a similar trend as the performances of each champion cells. According to the photovoltaic parameters presented in Table 2, the enhanced PCE in device with a BZACl additive is mainly attributed to the improvement of J_{SC} and FF. These results reveal that the BZACl additive provides the more efficient electron extraction and defect passivation than BZABr or BZAI. This is consistent with the passivation effect mentioned earlier in TRPL, XPS and EIS discussions. Notably, compared with the reference devices with the pristine perovskite film, the performances of the PSC devices with BZABr and BZAI additives

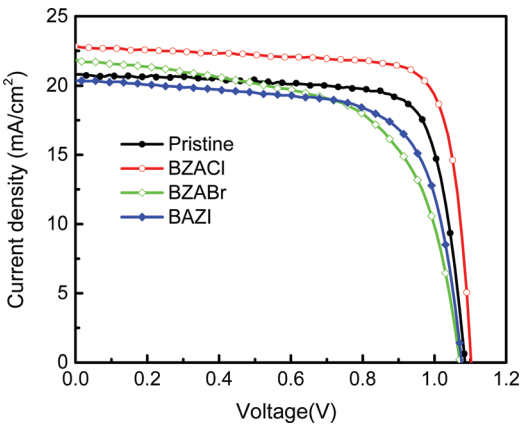

Fig. 8 *J–V* characteristics of the perovskite devices w/o and with various BZA halide salt additives in the perovskite layer under simulated AM 1.5G illumination.

even are worse with maximum PCE between 16.2% and 16.7%. This indicates that BZABr and BZAI additives cannot be efficient to passivate the defects in $MAPbI_3$. Thus, it can be seen that the organic BZA cation does not dominate the passivation.

Fig. 9(a) shows the external quantum efficiency (EQE), steady photocurrent output and stabilized PCE of the best-performing PSC device with BZACl additives. The integrated J_{SC} of 21.8 mA cm^{-2} from EQE is in good agreement with that from *J–V* measurement under the solar simulator within 5% deviation. In comparison with the pristine perovskite film, the PSC device with BZACl additives shows the increased EQE intensity along the entire range of wavelengths from 400 to 800 nm. It indicates that the light harvesting capability and charge extraction and collection can be effectively improved *via* incorporating BZACl additives. Besides, the stabilized PCE of the BZACl additive (see Fig. 9(b)) that measured at the maximum power point is 19.5%. It is almost identical to the PCE extracted from the *J–V* curve. In addition, the *J–V* characteristics of PSC device with BZACl additive was analysed in forward and reverse scanning directions under 100 mW cm^{-2} illumination to investigate the hysteresis effect. As shown in Fig. 9(c), the PCE is 19.8% in forward direction, with a V_{OC} of 1.10 V, a J_{SC} of 22.7 mA cm^{-2} and an FF of 79.3%, whereas PCE is 20.4% in the reverse direction, with a V_{OC} of 1.10 V, a J_{SC} of 23.2 mA cm^{-2} and an FF of 80.1%. Thus, the *J–V* curves from forward and reverse scanning directions almost overlap each other, which indicates a negligible hysteresis effect herein.

Finally, we evaluated the long-term stability of unencapsulated PSC devices with pristine perovskite films and with BZACl-doped perovskite films stored in an argon glovebox under ambient air conditions at room temperature (~45% relative humidity), respectively. As presented in Fig. 10, the PCE of the pristine-based device maintains 75% (100 days) and only 25% (30 days) of the initial value stored in an argon-filled glovebox under ambient air conditions, respectively. By contrast, the device with BZACl-doped perovskite films shows superior stability to the pristine-based device. In particular, it still can retain at least 90% of its initial PCE stored in ambient air after 30 days. This significantly enhanced stability indicates that the hydrophobic capping ligands of benzylammonium halide salts successfully prevent water from permeating the perovskite film and the chloride incorporation induces the effective defect passivation for stabilizing perovskite crystal structures. Table S3 (ESI†) provides a comparison of the photovoltaic performance and stability test of the inverted planar $MAPbI_3$ or $MAPbI_{3-x}Cl_x$ based PSCs with other additives in the literature. Herein, we defined these reports that the additive should be initially dissolved into the perovskite precursor solution for perovskite layer fabrication. As we noted, there were very few successful unencapsulated PSC devices, which can perform PCE approaching 20% and still have 90% retainment of its initial PCE after 30 days at ~45% relative humidity conditions. Therefore, we believe that our findings would offer a feasible and simple way to achieve the robust photoactive metal halide perovskite films *via* the further molecular design of arylammonium halide salts as additives.

Table 2 Photovoltaic performance parameters of devices w/o and with various BZA halide salt additives under simulated AM 1.5G illumination[ab]

	J_{sc} (mA cm^{-2})	V_{oc} (V)	FF (%)	PCE (%)
Pristine	20.9 ± 0.5 (21.8)	1.08 ± 0.01 (1.07)	75.2 ± 1.8 (75.7)	17.2 ± 0.4 (17.8)
BZACl	22.6 ± 0.1 (22.7)	1.08 ± 0.01 (1.10)	79.4 ± 0.6 (79.3)	19.2 ± 0.4 (19.8)
BZABr	20.9 ± 0.1 (21.0)	1.08 ± 0.03 (1.09)	69.0 ± 4.5 (71.2)	15.7 ± 0.4 (16.2)
BZAI	20.1 ± 1.5 (22.1)	1.07 ± 0.00 (1.08)	75.4 ± 4.6 (70)	16.3 ± 0.4 (16.7)

[a] The numbers in the brackets represent for the best-performing device. [b] Average performance from 20 devices.

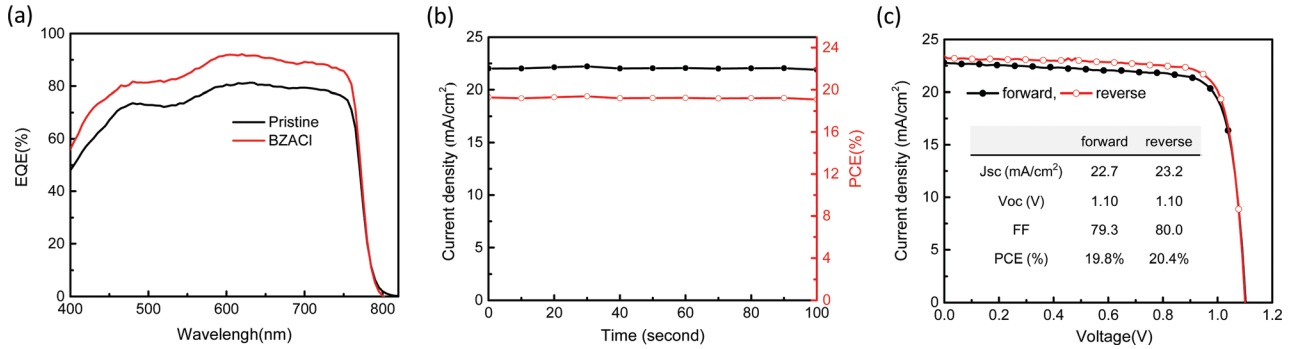

Fig. 9 (a) EQE spectra of perovskite devices with pristine perovskite films and BZACl additives. (b) steady-state J_{SC} and PCE and (c) J–V curves measured in the forward and reverse scan directions of perovskite devices with BZACl additives in the perovskite layer under simulated AM 1.5G irradiation.

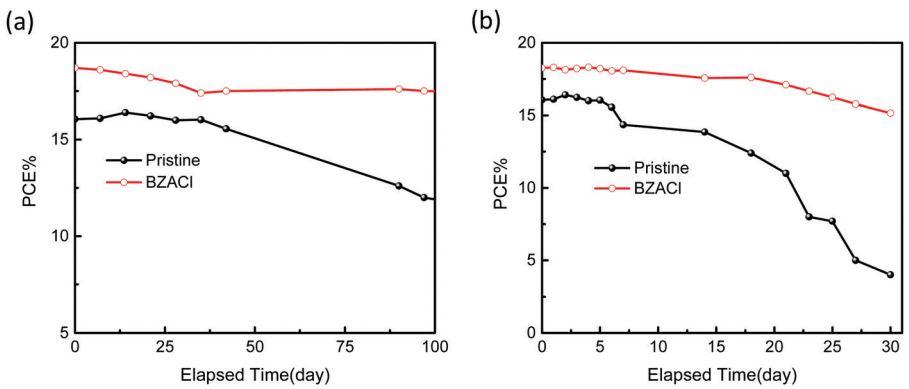

Fig. 10 Evolution of device stability for the unencapsulated PSCs w/o and with BZACl additives under (a) argon-filled glove box and (b) ambient air (~45% relative humidity) conditions, respectively.

Conclusions

In summary, we have introduced the additive engineering by using benzylammonium halide salts in inverted planar $MAPbI_3$-based perovskite solar cells. The steady-state PL and TRPL results have reasonably clarified the efficient defect passivation in the perovskite films by incorporating the benzylammonium halide salt additives. In particular, electrical impedance spectroscopy showed that the interfacial charge transfer resistance of the device with BZACl additives can be efficiently reduced, revealing more efficient electron extraction at the heterojunction interface. Consequently, a maximum efficiency of 19.8% and an average power conversion efficiency of 19.2%, as well as negligible hysteresis effects have been achieved for the device with BZACl additives. Meanwhile, it also greatly improves the long-term device moisture stability. Thus, our work provides the selection guide by utilizing arylammonium halide salts as additives for improving the power conversion efficiency and device long-term stability toward future photovoltaic industry applications.

Experimental section

Preparation of perovskite solar cells

Device fabrication. Indium tin oxide (ITO)-coated glass substrates (sheet resistance of 15 Ω sq^{-1}) were ultrasonically cleaned with an abstergent aqueous solution, deionized water, acetone, and isopropyl alcohol for 20 min and then, dried under a nitrogen (N_2) stream before use. Finally, the substrates

were cleaned with air plasma for 10 min. A NiO_x film ($\approx$20 nm) was prepared by spin-coating a solution containing NiO_x (nickel(II) acetylacetonate) dissolved in 5 mL of anhydrous ethanol with addition of 50 μL of 38% HCl. The NiO_x-coated substrates were then baked at 250 °C for 30 min in air. The $MAPbI_3$ precursor solution was obtained by dissolving 1.3 M PbI_2 and MAI (molar ratio of 1 : 1) in anhydrous DMF : DMSO (4 : 1). The additive solutions of benzylammonium halide salts were dissolved in anhydrous DMF at a concentration of 50 mg mL^{-1}. The appropriate volume (1 vol%) of additive solution was added into the perovskite precursor solution. The solution was stirred at 60 °C for 2 h in an argon glovebox. The perovskite precursor solutions without (w/o) and with benzylammonium halide salts (1 vol%) were spin coated onto NiO_x-coated substrates at Step-1 with 2000 rpm for 10 seconds and Step-2 with 4000 rpm for 20 seconds in the glovebox, and 250 μL of toluene was rapidly dropped onto the substrates to induce a fast crystallization after $\approx$6 seconds of spin coating. The perovskite precursor–coated substrate was dried on a hot plate at 100 °C for 10 minutes. Subsequently, the $PC_{61}BM$ (20 mg mL^{-1} in anhydrous chlorobenzene) was then sequentially deposited *via* spin coating at 2000 rpm for 30 seconds and the BCP (0.5 mg mL^{-1} in IPA) was then sequentially deposited *via* spin coating at 6000 rpm for 30 seconds. Finally, the device was completed upon the evaporation of Ag contact electrodes (100 nm) at a vacuum level of 10^{-7} Pa through a shadow mask. The active area of each device was 10 mm^2. All device measurements were performed in the ambient environment at room temperature, and the details of characterization were described in ESI.†

Conflicts of interest

There are no conflicts to declare.

Acknowledgements

This work is particularly supported by the independent post-doctoral research scholar funding at Ministry of Science and Technology, Taiwan (108-2113-M-002-019-MY3) and ''Aim for the Top University Plan'' of the National Taiwan University, the Ministry of Education, Taiwan (106R4000), research funding at Ministry of Science and Technology, Taiwan (107-2221-E-001-007-MY3, 106-2112-M-001-036-MY3).

References

1 T. M. Brenner, D. A. Egger, L. Kronik, G. Hodes and D. Cahen, Hybrid organic–inorganic perovskites: low-cost semiconductors with intriguing charge-transport properties, *Nat. Rev. Mater.*, 2016, **1**, 15007.
2 M. B. Johnston and L. M. Herz, Hybrid perovskites for photovoltaics: charge-carrier recombination, diffusion, and radiative efficiencies, *Acc. Chem. Res.*, 2016, **49**, 146–154.
3 S. D. Stranks, G. E. Eperon, G. Grancini, C. Menelaou, M. J. P. Alcocer, T. Leijtens, L. M. Herz, A. Petrozza and H. J. Snaith, Electron-hole diffusion lengths exceeding 1 micrometer in an organometal trihalide perovskite absorber, *Science*, 2013, **342**, 341–344.
4 J. Y. Kim, J. W. Lee, H. S. Jung, H. Shin and N. G. Park, High-efficiency perovskite solar cells, *Chem. Rev.*, 2020, **120**, 7867–7918.
5 https://www.nrel.gov/pv/cell-efficiency.html.
6 N. G. Park and K. Zhu, Scalable fabrication and coating methods for perovskite solar cells and solar modules, *Nat. Rev. Mater.*, 2020, **5**, 333–350.
7 H. Li and W. Zhang, Perovskite tandem solar cells: from fundamentals to commercial deployment, *Chem. Rev.*, 2020, **120**, 9835–9950.
8 C. Liu, Y. B. Cheng and Z. Ge, Understanding of perovskite crystal growth and film formation in scalable deposition processes, *Chem. Soc. Rev.*, 2020, **49**, 1653–1687.
9 I. A. Howard, T. Abzieher, I. M. Hossain, H. Eggers, F. Schackmar, S. Ternes, B. S. Richards, U. Lemmer and U. W. Paetzold, Coated and printed perovskites for photovoltaic applications, *Adv. Mater.*, 2019, **31**, 1806702.
10 J. W. Lee, D. K. Lee, D. N. Jeong and N. G. Park, Control of crystal growth toward scalable fabrication of perovskite solar cells, *Adv. Funct. Mater.*, 2019, **29**, 1807047.
11 C. Ran, J. Xu, W. Gao, C. Huang and S. Dou, Defects in metal triiodide perovskite materials towards high-performance solar cells: origin, impact, characterization, and engineering, *Chem. Soc. Rev.*, 2018, **47**, 4581–4610.
12 S. G. Motti, D. Meggiolaro, S. Martani, R. Sorrentino, A. J. Barker, F. DeAngelis and A. Petrozza, Defect activity in metal–halide perovskites, *Adv. Mater.*, 2019, **31**, 1901183.
13 A. F. Castro-Méndez, J. Hidalgo and J. P. Correa-Baena, The role of grain boundaries in perovskite solar cells, *Adv. Energy Mater.*, 2019, **9**, 1901489.
14 E. Aydin, M. DeBastiani and S. DeWolf, Defect and contact passivation for perovskite solar cells, *Adv. Mater.*, 2019, **31**, 1900428.
15 S. Akin, N. Arora, S. M. Zakeeruddin, M. Grätzel, R. H. Friend and M. I. Dar, New strategies for defect passivation in high-efficiency perovskite solar cells, *Adv. Energy Mater.*, 2020, **10**, 1903090.
16 S. M. Park, A. Abtahi, A. M. Boehm and K. R. Graham, Surface ligands for methylammonium lead iodide films: surface coverage, energetics,and photovoltaic performance, *ACS Energy Lett.*, 2020, **5**, 799–806.
17 H. Zhang, M. K. Nazeeruddin and W. C. H. Choy, Perovskite photovoltaics: the significant role of ligands in film formation, passivation, and stability, *Adv. Mater.*, 2019, **31**, 1805702.
18 Y. Lin, Y. Bai, Y. Fang, Z. Chen, S. Yang, X. Zheng, S. Tang, Y. Liu, J. Zhao and J. Huang, Enhanced thermal stability in perovskite solar cells by assembling 2D/3D stacking structures, *J. Phys. Chem. Lett.*, 2018, **9**, 654–658.
19 F. Zhang and K. Zhu, Additive engineering for efficient and stable perovskite solar cells, *Adv. Energy Mater.*, 2020, **10**, 1902579.
20 C. Li, A. Wang, L. Xie, X. Deng, K. Liao, J. A. Yang, T. Li and F. Hao, Emerging alkali metal ion (Li^+, Na^+, K^+ and Rb^+)

doped perovskite films for efficient solar cells: recent advances and prospects, *J. Mater. Chem. A*, 2019, **7**, 24150–24163.

21 L. Jia, M. Chen and S. Yang, Functionalization of fullerene materials toward applications in perovskite solar cells, *Mater. Chem. Front.*, 2020, **4**, 2256–2282.

22 R. Wang, J. Xue, L. Meng, J. W. Lee, Z. Zhao, P. Sun, L. Cai, T. Huang, Z. Wang, Z. K. Wang, Y. Duan, J. L. Yang, S. Tan, Y. Yuan, Y. Huang and Y. Yang, Caffeine improves the performance and thermal stability of perovskite solar cells, *Joule*, 2019, **3**, 1464–1477.

23 J. Feng, X. Zhu, Z. Yang, X. Zhang, J. Niu, Z. Wang, S. Zuo, S. Priya, S. Liu and D. Yang, Record sfficiency stable flexible perovskite solar cell using effective additive assistant strategy, *Adv. Mater.*, 2018, **30**, 1801418.

24 D. S. Lee, J. S. Yun, J. Kim, A. M. Soufiani, S. Chen, Y. Cho, X. Deng, J. Seidel, S. Lim, S. Huang and A. W. Y. Ho-Baillie, Passivation of grain boundaries by phenethylammonium in formamidinium-methylammonium lead halide perovskite solar cells, *ACS Energy Lett.*, 2018, **3**, 647–654.

25 J. Cheng, H. Zhang, S. Zhang, D. Ouyang, Z. Huang, M. K. Nazeeruddin, J. Hou and W. C. H. Choy, Highly efficient planar perovskite solar cells achieved by simultaneous defect engineering and formation kinetic control, *J. Mater. Chem. A*, 2018, **6**, 23865–23874.

26 J. Yang, C. Liu, C. Cai, X. Hu, Z. Huang, X. Duan, X. Meng, Z. Yuan, L. Tan and Y. Chen, High-performance perovskite solar cells with excellent humidity and thermo-stability via fluorinated perylenediimid, *Adv. Energy Mater.*, 2019, **9**, 1900198.

27 T. Wu, Y. Wang, X. Li, Y. Wu, X. Meng, D. Cui, X. Yang and L. Han, Efficient defect passivation for perovskite solar cells by controlling the electron density distribution of donor-π-acceptor molecules, *Adv. Energy Mater.*, 2019, **9**, 1803766.

28 S. Bai, P. Da, C. Li, Z. Wang, Z. Yuan, F. Fu, M. Kawecki, X. Liu, N. Sakai, J. T. W. Wang, S. Huettner, S. Buecheler, M. Fahlman, F. Gao and H. J. Snaith, Planar perovskite solar cells with long-term stability using ionic liquid additives, *Nature*, 2019, **571**, 245–250.

29 X. Zheng, Y. Deng, B. Chen, H. Wei, X. Xiao, Y. Fang, Y. Lin, Z. Yu, Y. Liu, Q. Wang and J. Huang, Dual functions of crystallization control and defect passivation enabled by sulfonic zwitterions for stable and efficient perovskite solar cells, *Adv. Mater.*, 2018, **30**, 1803428.

30 Y. Y. Yu, C. Tseng, W. C. Chien, H. L. Hsu and C. P. Chen, Photovoltaic performance enhancement of perovskite solar cells using polyimide and polyamic acid as additives, *J. Phys. Chem. C*, 2019, **123**, 23826–23833.

31 Z. Huang, X. Hu, C. Liu, L. Tan and Y. Chen, Nucleation and crystallization control *via* polyurethane to enhance the bendability of perovskite solar cells with excellent device performance, *Adv. Funct. Mater.*, 2017, **27**, 1703061.

32 T. Li, Y. Pan, Z. Wang, Y. Xia, Y. Chen and W. Huang, Additive engineering for highly efficient organic–inorganic halide perovskite solar cells: recent advances and perspectives, *J. Mater. Chem. A*, 2017, **5**, 12602–12652.

33 S. Liu, Y. Guan, Y. Sheng, Y. Hu, Y. Rong, A. Mei and H. Han, A review on additives for halide perovskite solar cells, *Adv. Energy Mater.*, 2020, **10**, 1902492.

34 Y. Bai, Y. Lin, L. Ren, X. Shi, E. Strounina, Y. Deng, Q. Wang, Y. Fang, X. Zheng, Y. Lin, Z. G. Chen, Y. Du, L. Wang and J. Huang, Oligomeric silica-wrapped perovskites enable synchronous defect passivation and grain stabilization for efficient and stable perovskite photovoltaics, *ACS Energy Lett.*, 2019, **4**, 1231–1240.

35 S. Fu, X. Li, L. Wan, Y. Wu, W. Zhang, Y. Wang, Q. Bao and J. Fang, Efficient passivation with lead pyridine-2-carboxylic for high-performance and stable perovskite solar cells, *Adv. Energy Mater.*, 2019, **9**, 1901852.

36 F. Huang, M. Li, P. Siffalovic, G. Cao and J. Tian, From scalable solution fabrication of perovskite films towards commercialization of solar cells, *Energy Environ. Sci.*, 2019, **12**, 518–549.

37 F. Wang, W. Geng, Y. Zhou, H. H. Fang, C. J. Tong, M. A. Loi, L. M. Liu and N. Zhao, Phenylalkylamine passivation of organolead halide perovskites enabling high-efficiency and air-stable photovoltaic cells, *Adv. Mater.*, 2016, **28**, 9986–9992.

38 Y. Liu, S. Akin, L. Pan, R. Uchida, N. Arora, J. V. Milić, A. Hinderhofer, F. Schreiber, A. R. Uhl, S. M. Zakeeruddin, A. Hagfeldt, M. Ibrahim Dar and M. Grätzel, Ultrahydrophobic 3D/2D fluoroarene bilayer-based water-resistant perovskite solar cells with efficiencies exceeding 22%, *Sci. Adv.*, 2019, **5**, 2543.

39 G. Liu, H. Zheng, H. Xu, L. Zhang, X. Xu, S. Xu and X. Pan, Interface passivation treatment by halogenated low-dimensional perovskites for high-performance and stable perovskite photovoltaics, *Nano Energy*, 2020, **73**, 104753.

40 P. Y. Gu, N. Wang, A. Wu, Z. Wang, M. Tian, Z. Fu, X. W. Sun and Q. Zhang, An azaacene derivative as promising electron-transport layer for inverted perovskite solar cells, *Chem. – Asian J.*, 2016, **11**, 2135–2138.

41 A. A. Said, J. Xie and Q. Zhang, Recent progress in organic electron transport materials in inverted perovskite solar cells, *Small*, 2019, **15**, 1900854.

42 M. L. Agiorgousis, Y. Sun, H. Zeng and S. Zhang, Strong covalency-induced recombination centers in perovskite solar cell material $CH_3NH_3PbI_3$, *J. Am. Chem. Soc.*, 2014, **136**, 14570–14575.

43 W. Li, Y. Y. Sun, L. Li, Z. Zhou, J. Tang and O. V. Prezhdo, Control of charge recombination in Perovskites by Oxidation State of Halide Vacancy, *J. Am. Chem. Soc.*, 2018, **140**, 15753–15763.

44 Q. Chen, H. Zhou, Y. Fang, A. Z. Stieg, T. BinSong, H. H. Wang, X. Xu, Y. Liu, S. Lu, J. You, P. Sun, J. McKay, M. S. Goorsky and Y. Yang, The optoelectronic role of chlorine in $CH_3NH_3PbI_3$(Cl)-based perovskite solar cells, *Nat. Commun.*, 2015, **6**, 7269.

45 M. Wang, B. Li, J. Yuan, F. Huang, G. Cao and J. Tian, Repairing defects of halide perovskite films To enhance photovoltaic performance, *ACS Appl. Mater. Interfaces*, 2018, **10**, 37005–37013.

46 M. I. Saidaminov, J. Kim, A. Jain, R. Quintero-Bermudez, H. Tan, G. Long, F. Tan, A. Johnston, Y. Zhao, O. Voznyy and E. H. Sargent, Suppression of atomic vacancies via incorporation of isovalent small ions to increase the stability of halide perovskite solar cells in ambient air, *Nat. Energy*, 2018, **3**, 648–654.

47 M. J. P. Alcocer, T. Leijtens, L. M. Herz, A. Petrozza and H. J. Snaith, Electron-hole diffusion lengths exceeding 1 micrometer in an organometal trihalide perovskite absorber, *Science*, 2013, **342**, 341–344.

48 K. Odysseas Kosmatos, L. Theofylaktos, E. Giannakaki, D. Deligiannis, M. Konstantakou and T. Stergiopoulos, Methylammonium chloride: a key additive for highly efficient, stable, and up-scalable perovskite solar cells, *Energy Environ. Mater.*, 2019, **2**, 79–92.

49 T. Baikie, Y. Fang, J. M. Kadro, M. Schreyer, F. Wei, S. G. Mhaisalkar, M. Graetzel and T. J. White, Synthesis and crystal chemistry of the hybrid perovskite $(CH_3NH_3)PbI_3$ for solid-state sensitised solar cell applications, *J. Mater. Chem. A*, 2013, **1**, 5628–5641.

50 L. N. Quan, M. Yuan, R. Comin, O. Voznyy, E. M. Beauregard, S. Hoogland, A. Buin, A. R. Kirmani, K. Zhao, A. Amassian, D. H. Kim and E. H. Sargent, ligand-stabilized reduced-dimensionality perovskites, *J. Am. Chem. Soc.*, 2016, **138**, 2649–2655.

51 K. H. Stone, A. Gold-Parker, V. L. Pool, E. L. Unger, A. R. Bowring, M. D. McGehee, M. F. Toney and C. J. Tassone, Transformation from crystalline precursor to perovskite in $PbCl_2$-derived $MAPbI_3$, *Nat. Commun.*, 2018, **9**, 3458.

52 D. P. Nenon, J. A. Christians, L. M. Wheeler, J. L. Blackburn, E. M. Sanehira, B. Dou, M. L. Olsen, K. Zhu, J. J. Berry and J. M. Luther, Structural and chemical evolution of methylammonium lead halide perovskites during thermal processing from solution, *Energy Environ. Sci.*, 2016, **9**, 2072–2082.

53 S. P. Harvey, J. Messinger, K. Zhu, J. M. Luther and J. J. Berry, Investigating the effects of chemical gradients on performance and reliability within perovskite solar cells with TOF-SIMS, *Adv. Energy Mater.*, 2020, **10**, 1903674.

54 T. Kirchartz, J. A. Márquez, M. Stolterfoht and T. Unold, Photoluminescence-based characterization of halide perovskites for photovoltaics, *Adv. Energy Mater.*, 2020, **10**, 1904134.

55 T. H. Han, J. W. Lee, C. Choi, S. Tan, C. Lee, Y. Zhao, Z. Dai, N. DeMarco, S. J. Lee, S. H. Bae, Y. Yuan, H. M. Lee, Y. Huang and Y. Yang, Perovskite-polymer composite cross-linker approach for highly-stable and efficient perovskite solar cells, *Nat. Commun.*, 2019, **10**, 520.

56 Y. Wu, X. Li, S. Fu, L. Wan and J. Fang, Efficient methylammonium lead trihalide perovskite solar cells with chloroformamidinium chloride (Cl-FACl) as an additive, *J. Mater. Chem. A*, 2019, **7**, 8078–8084.

57 H. Jiang, Z. Yan, H. Zhao, S. Yuan, Z. Yang, J. Li, B. Liu, T. Niu, J. Feng, Q. Wang, D. Wang, H. Yang, Z. Liu and S. F. Liu, Bifunctional hydroxylamine hydrochloride incorporated perovskite films for efficient and stable planar perovskite solar cells, *ACS Appl. Energy Mater*, 2018, **1**, 900–909.

58 S. Ali, S. Chang, M. Imran, Q. Shi, Y. Chen and H. Zhong, Impedance spectroscopy: a versatile technique to understand solution-processed optoelectronic devices, *Phys. Status Solidi RRL*, 2019, **13**, 1800580.

59 X. Huang, H. Guo, K. Wang and X. Liu, Ionic liquid induced surface trap-state passivation for efficient perovskite hybrid solar cells, *Org. Electron.*, 2017, **41**, 42–48.

60 M. Sasikumar, G. Maddala, M. Ambapuram, M. Subburu, J. R. Vaidya, S. N. Babu, P. Chetti, R. Mitty and S. Pola, Cost-effective thiophene-assisted novel dopantfree hole transport materials for efficient perovskite solar cell performance, *Sustainable Energy Fuels*, 2020, **4**, 4754–4767.